HIGH RESOLUTION PIV MEASUREMENTS OF AN IMPINGING UNDEREXPANDED SUPERSONIC JET

Omid Amili
Laboratory for Turbulence Research in Aerospace and Combustion,
Department of Mechanical and Aerospace Engineering, Monash University, Melbourne, Australia
omid.amili@monash.edu

Daniel Edgington-Mitchell
Laboratory for Turbulence Research in Aerospace and Combustion,
Department of Mechanical and Aerospace Engineering, Monash University, Melbourne, Australia
daniel.mitchell@monash.edu

Damon Honnery
Laboratory for Turbulence Research in Aerospace and Combustion,
Department of Mechanical and Aerospace Engineering, Monash University, Melbourne, Australia
damon.honnery@monash.edu

Julio Soria
Laboratory for Turbulence Research in Aerospace and Combustion,
Department of Mechanical and Aerospace Engineering, Monash University, Melbourne, Australia
Department of Aeronautical Engineering, King Abdulaziz University,
Jeddah 21589, Kingdom of Saudi Arabia
julio.soria@monash.edu

ABSTRACT

PIV measurements of the velocity field of a supersonic jet impinging on a flat surface were conducted for a pure convergent nozzle with a nozzle pressure ratio of NPR=3.4 and a nozzle to plate spacing of $Z/D = 5.0$. The velocity field at a center plane of the jet was resolved at a high-spatial resolution of $0.012D$ in the streamwise and radial directions. The paper reports the complex flow structure as well as the lower- and higher-order statistics.

INTRODUCTION

The physics of supersonic jets has been under investigation over the last five decades due to their various aerospace and industrial applications. When a jet exits a nozzle with a pressure higher than the pressure of the surrounding area, an underexpanded jet forms. This pressure mismatch generates a series of shock and expansion waves within the jet core. This situation becomes more complicated when the jet interacts with an impingement surface. Understanding of the impinging jet flow is important in the design and control of short vertical takeoff and landing (SVTOL) of aircrafts, rocket/missile launching systems (Henderson, 2002; Kumar *et al.*, 2013), and in the cold spray coating process (Gilmore *et al.*, 1999; Assadi *et al.*, 2003).

The flow field in supersonic impinging jets is typically highly unsteady. It contains a feedback loop that was first described by Powell (1953). This mechanism is initiated by instabilities in the shear layer at the nozzle lip. The instability waves grow in size and evolve into large scale vortical structures that convect downstream. Near the plate surface, these large scale structures interact with the stand-off shock formed above the plate. This interaction produces motion in the wall jet, and this motion in turn generates an impulsive acoustic wave that propagates back to the nozzle lip (Henderson *et al.*, 2005). At the nozzle lip, these acoustic waves force the shear layer, creating the incipient instability waves and thus completing the feedback loop. Henderson (2002) and others have however demonstrated that “zones of silence” exist; at some conditions the jet exhibits no feedback loop.

The authors have previously shown the cyclic nature of the impingement process and the closed loop instability mechanisms using two sets of high-spatial and high-temporal resolution schlieren images of an impinging jet (Buchmann *et al.*, 2011; Mitchell *et al.*, 2012). Figure 1 visualizes the acoustic waves traveling towards the nozzle and the coherent structures at the shear layer. In the present study, high-spatial resolution measurements of the velocity fields of this phenomenon are reported. The important parameters that affect the flow structure and noise production are the nozzle pressure ratio (NPR), the nozzle to surface

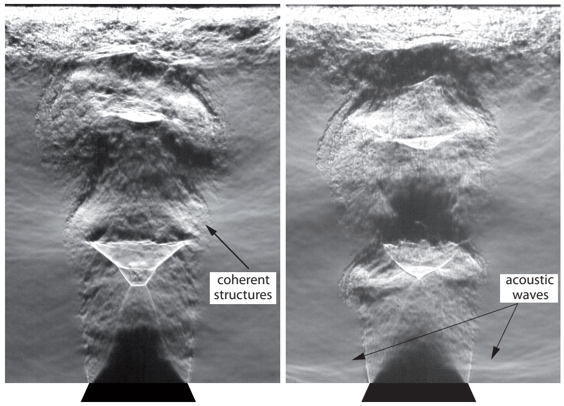

Figure 1: Instantaneous high-spatial resolution schlieren images of $d\rho/dx$ representing the acoustic waves and coherent structures in a feedback loop mechanism for NPR=3.2, and Z/D=4.0 (Mitchell *et al.*, 2012).

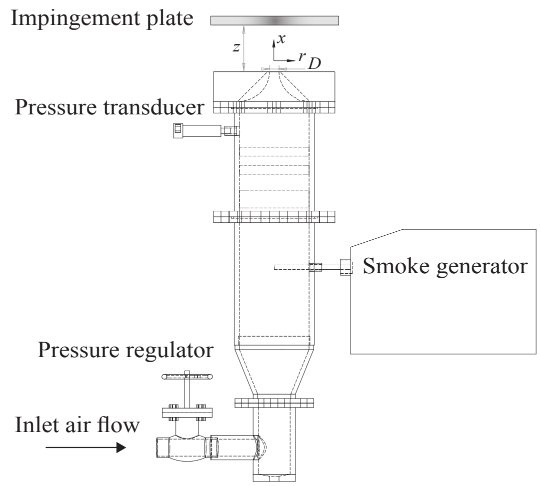

Figure 2: A schematic diagram of the experimental facility.

spacing (stand-off distance), the Reynolds number, the nozzle shape, and the impinging plate's size and angle.

The flow regime, instabilities, coherent structures, and the generated noise level are functions of the above parameters, especially the NPR and the stand-off distance. The sensitivity of the jet behaviour to certain operating parameters is illustrated in Kumar *et al.* (2013). The authors demonstrated for an impinging jet at Z/D=4.0 with nozzle pressure ratio of 3.7, the shear layer is dominated by helical instabilities, where a micro jet noise suppression mechanism was shown to be be quite effective. However, for Z/D=4.5 at the same NPR, the flow is dominated by strong coherent axisymmetric structures where the same noise control mechanism is ineffective. As a result, it is important to address this fundamental problem at different operating conditions.

In the present study, the high-spatial resolution 2C-2D PIV measurements are performed along the streamwise-radial direction at a center plane of the jet. Nozzle pressure ratios ranging between 2 to 5 with stand-off distances in the range of 1-5 are investigated. The paper is aimed at addressing the flow structure and lower- and higher-order statistics only for the nozzle pressure ratio of 3.4 and the stand-off distance of 5.0.

EXPERIMENTAL METHODOLOGY

Jet rig facility

The apparatus used in this study was designed and developed based on the performance of an earlier LTRAC Supersonic Jet Facility (Mitchell *et al.*, 2013). Compressed air at a pressure of approximately 7 bar and a temperature of approximately 20 ^{o}C is transferred from the supply line into the mixing chamber of the jet facility using a high-pressure hose. The inlet compressed flow is regulated using a Fairchild (0-10 bar) high-flow pressure regulator with a pressure variation of approximately 1%. The flow temperature was monitored using several thermocouples. The mixing chamber with wire mesh at both ends is connected to a plenum chamber that contains a honeycomb section followed by wire meshes. This ensures that the flow is straightened before entering the nozzle. The stagnation pressure in the plenum chamber is measured using a RS-461 pressure transducer with an accuracy of approximately 0.25%. In this experiment, a converging nozzle with the inner exit diameter of 15 mm is mounted on the top of the plenum chamber. The nozzle which was manufactured using CNC machining of a single stainless steel block, has a sharp lip with a thickness of 1.5 mm. A machined insert as shown in Figure 2 is used to cover the outer region of the nozzle. A square piece of glass with a size of $15D\times15D$ is used as the impinging surface where D is the nozzle exit diameter. For seeding, a Vicount 1300 smoke generator is connected to the mixing chamber as shown in Figure 2. The smoke generator provides a persistent and high seeding density with a nominal particle size of 0.2$\sim$0.3 μm. In order to have a better seeding outcome and to decrease the chance of oil condensation and hence formation of large droplets, the smoke is additionally heated in a in-house heat exchanger before its entrance to the vessel. The particle relaxation time of approximately 2.0 μs is calculated experimentally based on the approach described in Mitchell *et al.* (2013). The corresponding effective particle diameter is approximately 0.6 μm. A schematic diagram of the experimental facility is shown in Figure 2. The Reynolds number based on the jet's ideally expanded velocity and the nozzle exit diameter is approximately 4.5×10^5. The Reynolds number at the nozzle exit is approximately 7.6×10^5. The isentropic flow assumption is used to calculate the pressure and the temperature at the jet exit.

Optical setup-PIV analysis

The application of particle image velocimetry (PIV) to supersonic flows is accompanied with several challenges as described by Scarano (2008); Mitchell *et al.* (2011). However, upon addressing the issues, PIV can be a reliable measuring tool in this type of jet flow. In this study, a two-cavity Nd:YAG pulsed laser (532 nm and 200 mJ per pulse) is used as the illumination source. An appropriate combination of spherical and cylindrical lenses is used to reduce the beam diameter and to produce a collimated laser sheet with a thickness of approximately 1 mm. Two 12-bit Imperx B6640 cameras with a CCD array of 6,600 px $\times$4,400 px and a pixel size of 5.5μm$\times$5.5μm are used as the imaging sensors. The use of 200 mm Micro-Nikkor lenses yielded

Table 1: PIV parameters

Parameter	Physical unit	Non-dim. unit	Physical unit	Non-dim. unit
	Camera 1		Camera 2	
Img. resolution	11.84μm/px	–	6.87μm/px	–
Diffraction limited dia.	$\sim$11μm	–	$\sim$13μm	–
Field of view*	78mm $\times$ 52mm	5.2D $\times$ 3.5D	45mm $\times$ 30mm	3.0D $\times$ 2.0D
Depth of field	$\sim$810μm	$\sim$0.05D	$\sim$410μm	$\sim$0.03D
IW_0*	128px $\times$ 64px	0.1 $\times$ 0.05	160px $\times$ 64px	0.6 $\times$ 0.03
IW_1	32px $\times$ 32px	0.025D $\times$ 0.025D	32px $\times$ 32px	0.015D $\times$ 0.015D
Vector spacing	16px $\times$ 16px	0.012D $\times$ 0.012D	16px $\times$ 16px	0.007D $\times$ 0.007D
Time delay	$\sim$880ns	–	$\sim$880ns	–

* along the streamwise and radial directions respectively.

magnifications of approximately 0.46 and 0.8. A F-number of 5.6 was used in the both cases. The first imaging system with the larger field of view was used to measure the entire stand-off distance and the second system was used to zoom in at a location between the first and second shock cells. A reliable control system developed at LTRAC was used to generate high-precession triggering signals (Fedrizzi & Soria, 2015). The jitter of laser pulses that was monitored using a photodiode was as low as 4ns. 10,000 image pairs were recorded at a rate of 1.0 Hz simultaneously for the both configurations. Due to the small size of particles, the diffraction limited diameter dominates the particle's geometric size. The depth of field estimation given in Table 1 is based on the diffraction limited image diameter, F-number, and the magnification (Raffel *et al.*, 2007). For the cross correlation of the image pairs, multi-grid cross-correlation digital particle image velocimetry (MCCDPIV) algorithm developed by Soria (1996) was employed. Multi-passing with a small final interrogation window at a high sub-pixel accuracy (using 2D Gaussian peak-fitting function) enables measurements with a high dynamic range. The PIV parameters are shown in Table 1.

RESULTS

Figure 3 shows the velocity magnitude of an instantaneous field. The streamlines are shown in order to better visualize the air entrainment into the shear layer and the formation of the wall jet at the impingement surface. The normalization is done using the jet exit velocity (U_e) that is approximately 315 m/s.

As can be seen, fine flow features are well resolved. Important flow features that cannot necessarily be inferred from the mean fields are highlighted in this figure. The visual inspection of instantaneous velocity fields shows the existence of stagnation/low-speed regions after the shock cells in the jet potential core especially after the first shock. A higher spatial resolution measurement that was performed simultaneously with the full domain measurement confirms the existence of these regions. At this stage, the authors believe that this phenomenon is related to the formation and disruption of the Mach disk at this specific operating and boundary condition. A stagnation bubble forms, speeds up, convects downstream, and interacts with the following shock cell. A sequence of this plausible scenario is shown in Figures 4. Velocity in this region at an early stage as shown in Figure 4(a) is very close to zero. As the region speeds up, it grows in size, and moves towards the second shock cell. Similar regions are noticed after the second shock, but they are not as strong as shown in Figure 4. It is worth emphasizing that the measurements are not phased-locked, and hence this sequence does not belong to a single low-speed event. This phenomenon was not noticed when the impingement plate was removed that shows the link between the occurrence of this event and the solid surface. Along with this, Edgington-Mitchell *et al.* (2014*a*) using a triple decomposition by Proper Orthogonal Decomposition showed that there is no recirculation zone in the Mach disk for a free jet. Further investigation is required to understand the mechanism behind the formation of the stagnation region and to learn if this plays an important role in the feedback loop mechanism and in the flow structure.

Figure 5 shows the mean and fluctuating components of the axial and radial velocities at the center plane of the jet. Flow statistics are symmetric along the jet centerline due to the fact that the experiment was performed with extreme caution and a large number of samples was collected. It is worth noting that the sample size is large enough so that the convergence of the first to fourth-order statistics was confirmed within the measurement uncertainty.

A periodic shock cell structure is evident from the variation of both the mean axial (Figure 5a) and radial velocity (Figure 5c) maps. Figure 6 shows the mean and the fluctuation of the axial velocity along the jet centerline, near the shear layer, and outside the potential core. The spacing between the peaks or valleys in the mean profile represents the shock cell spacing. The oscillation of the u_{rms} along the centerline also reflects the position of the shock cells. Outside the core of the jet, the RMS profile has a monotonic growth towards the impingement plate where in the vicinity of the plate it starts to decline. Along the shear layer, there is not a monotonic growth, but oscillations that are related to the reflection points of the shock waves at the shear layer.

In Figure 5(b), regions with high-level of turbulence is noticed near the shear layer and at the location of the shock cells indicating of a highly resonant and unsteady

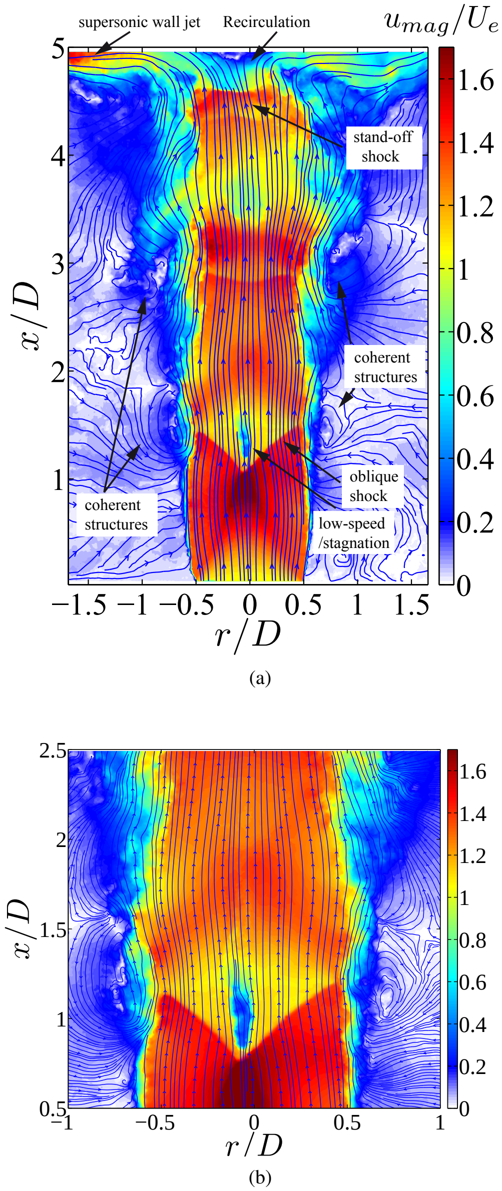

Figure 3: An instantaneous velocity field for (a) the entire field of view (camera 1) (b) zoomed-in area (camera 2).

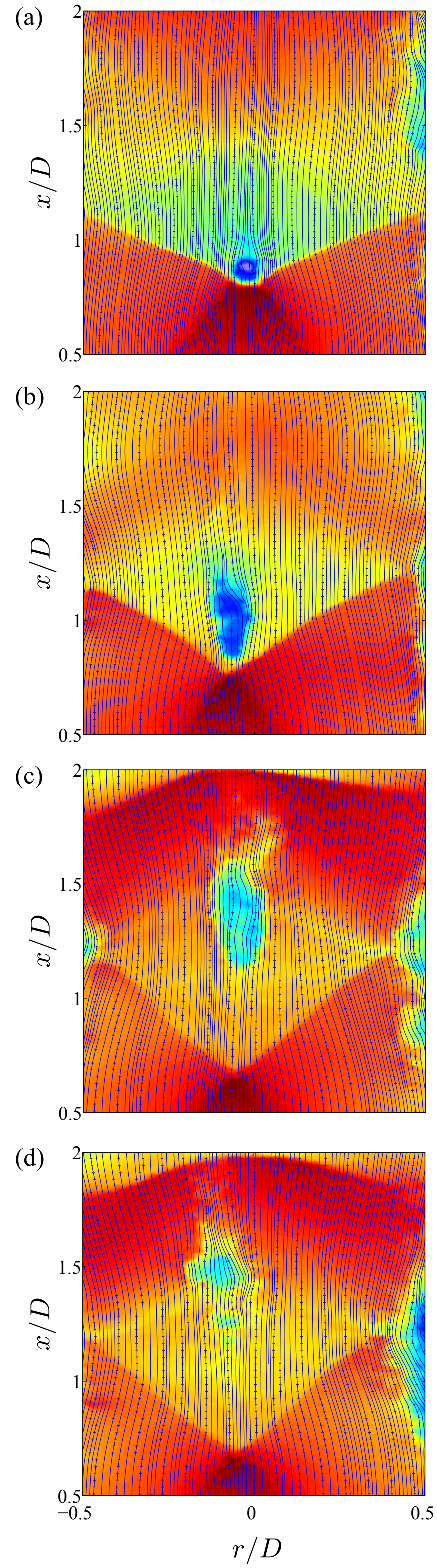

Figure 4: A plausible trend (from a to d) for the formation and development of a subsonic region located between the first and the second shock cells. For the color coding, see Figure 3.

phenomenon occurring there. It is worth highlighting that the oscillating motion of the shock cell specifically along the jet axis increases the fluctuations of the streamwise velocity component. That is more evident for shocks closer to the impingement surface. As shown previously, transverse motions of the shock waves may introduce axial oscillations (Edgington-Mitchell *et al.*, 2014*b*). Note that the artificial fluctuations imposed by the measurement also contribute to this, see Mitchell *et al.* (2013) for further details. Figure 5(e) shows the mean azimuthal component of the vorticity normalized by the nozzle exit diameter and the jet exit velocity. The maxima of the mean out-of-plane vorticity occurs at the shear layer near the jet exit with similar levels at two sides of the jet. As clear from the contour, the vorticity sign changes when the jet hits the wall.

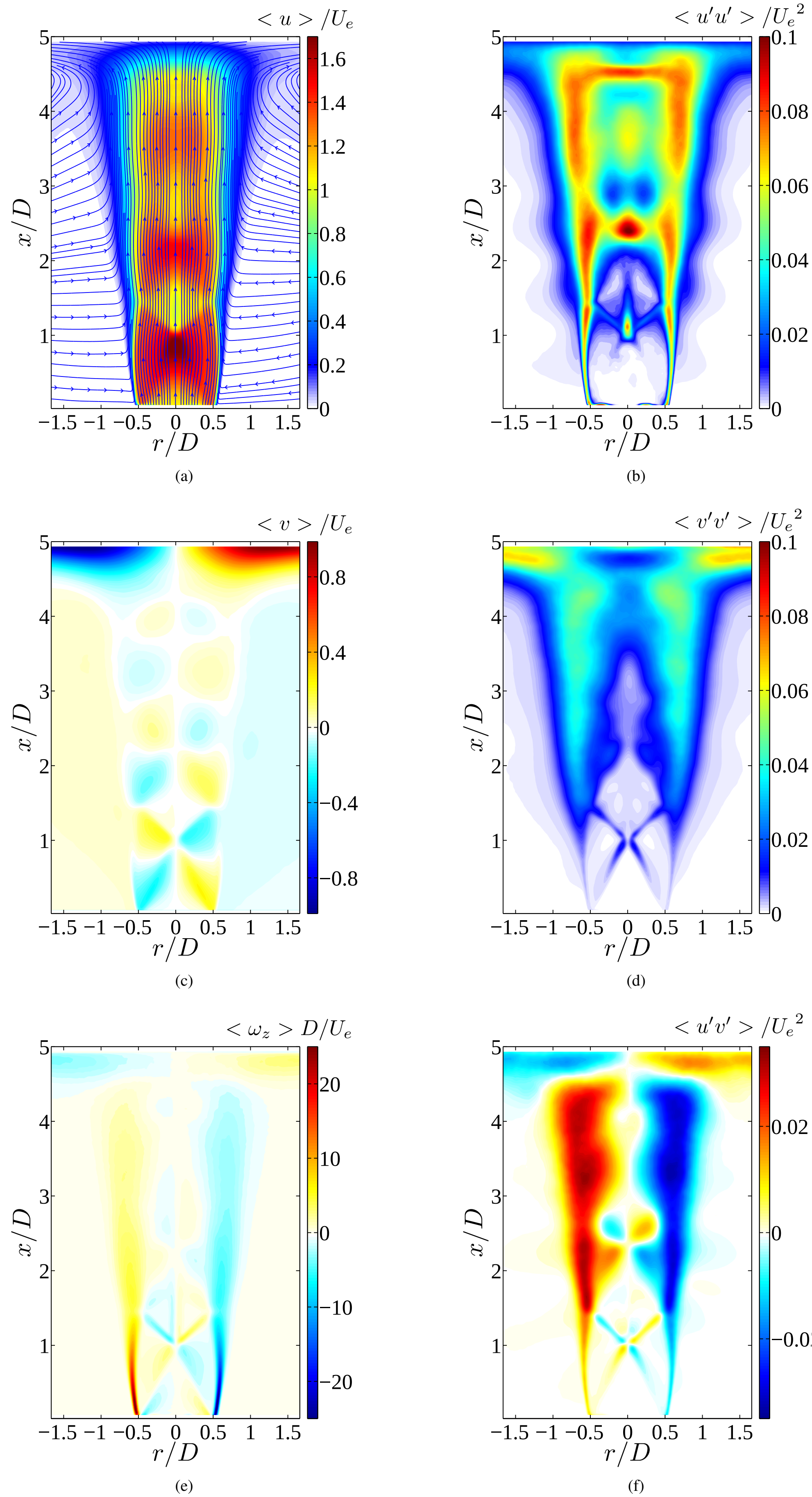

Figure 5: First- and second-order statistics.

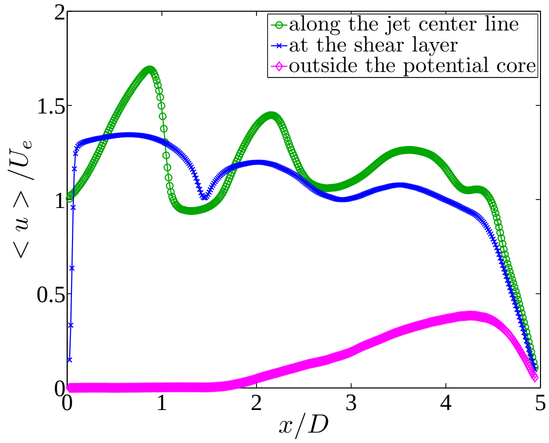

(a)

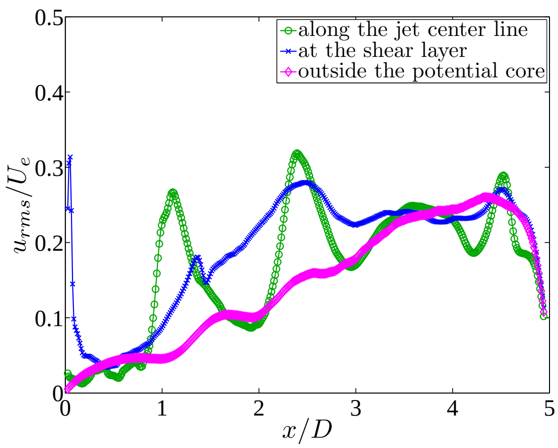

(b)

Figure 6: (a) Mean and (b) RMS of the axial velocity along the centerline of the jet, at the shear layer, and outside the potential core of the jet.

CONCLUDING REMARKS

An ultra high-spatial resolution measurement of an impinging supersonic jet at a nozzle pressure ratio of 3.4 and a stand-off distance of 5 was performed. The complex flow structure that is a resultant of interaction of the jet with the impingement surface and acoustic field was investigated. Fine flow features that are well resolved were discussed including the formation of a low-speed region after the first shock cell. A stagnation bubble forms, speeds up, convects downstream, and interacts with the following shock cell. This event is possibly linked to the formation and break up of the Mach disk at certain operating conditions.

Acknowledgment

The financial support to conduct this research by the Australian Research Council is gratefully acknowledged. This research was undertaken with the assistance of resources from the National Computational Infrastructure (NCI), which is supported by the Australian Government.

REFERENCES

Assadi, H., Gärtner, F., Stoltenhoff, T. & Kreye, H. 2003 Bonding mechanism in cold gas spraying. *Acta Materialia* **51** (15), 4379–4394.

Buchmann, N. A., Mitchell, D., Ingvorsen, K. M., Honnery, D. & Soria, J. 2011 High spatial resolution imaging of a supersonic underexpanded jet impinging on a flat plate. In *Sixth Australian Conference on Laser Diagnostics in Fluid Mechanics and Combustion, Canberra, Australia, 57 December, 2011*.

Edgington-Mitchell, D., Honnery, D.R. & Soria, J. 2014*a* The underexpanded jet mach disk and its associated shear layer. *Physics of Fluids* **26** (9).

Edgington-Mitchell, D., Oberleithner, K., Honnery, D. & Soria, J. 2014*b* Coherent structure and sound production in the helical mode of a screeching axisymmetric jet. *Journal of Fluid Mechanic* **748**, 822–847.

Fedrizzi, M. & Soria, J. 2015 Application of a single-board computer as a low cost pulse generator. *Measurement Science & Technology* **under review**.

Gilmore, D.L., Dykhuizen, R.C., Neiser, R.A., Roemer, T.J. & Smith, M.F. 1999 Particle velocity and deposition efficiency in the cold spray process. *Journal of Thermal Spray Technology* **8** (4), 576–582.

Henderson, B. 2002 The connection between sound production and jet structure of the supersonic impinging jet. *Journal of the Acoustical Society of America* **111** (2), 735–747.

Henderson, B., Bridges, J. & Wernet, M. 2005 An experimental study of the oscillatory flow structure of tone-producing supersonic impinging jets. *Journal of Fluid Mechanics* **542**, 115–137.

Kumar, R., Wiley, A., Venkatakrishnan, L. & Alvi, F. 2013 Role of coherent structures in supersonic impinging jets. *Physics of Fluids* **25** (7).

Mitchell, D., Honnery, D. & Soria, J. 2011 Particle relaxation and its influence on the particle image velocimetry cross-correlation function. *Experiments in Fluids* **51** (4), 933–947.

Mitchell, D.M., Honnery, D.R. & Soria, J. 2012 The visualization of the acoustic feedback loop in impinging underexpanded supersonic jet flows using ultra-high frame rate schlieren. *Journal of Visualization* **15** (4), 333–341.

Mitchell, D.M., Honnery, D.R. & Soria, J. 2013 Near-field structure of underexpanded elliptic jets. *Experiments in Fluids* **54** (7).

Powell, A. 1953 On edge tones and associated phenomena. *Acoustica* **3**, 233–243.

Raffel, M., Willert, C.E., Wereley, S.T. & Kompenhans, J. 2007 *Particle Image Velocimetry, A Practical Guide*, 2^{nd} ed. edn. Springer.

Scarano, F. 2008 *Particle Image Velocimetry*, *Springer*, vol. 112, chap. Overview of PIV in Supersonic Flows, pp. 445–463.

Soria, J. 1996 An investigation of the near wake of a circular cylinder using a video-based digital cross-correlation particle image velocimetry technique. *Experimental Thermal and Fluid Science* **12** (2), 221–233.